Electrochimica Acta 54 (2009) 5583–5592

Contents lists available at ScienceDirect

Electrochimica Acta

journal homepage: www.elsevier.com/locate/electacta

Modelling and simulations of carbon corrosion during operation of a Polymer Electrolyte Membrane fuel cell

Jingwei Hu [a], P.C. Sui [a,*], Sanjiv Kumar [b], Ned Djilali [a]

[a] Institute for Integrated Energy Systems, University of Victoria, PO Box 3055 STN CSC, Victoria, BC V8W 3P6, Canada
[b] Ballard Power Systems, 9000 Glenlyon Parkway, Burnaby, BC V5J 5J8, Canada

ARTICLE INFO

Article history:
Received 12 March 2009
Received in revised form 23 April 2009
Accepted 24 April 2009
Available online 13 May 2009

Keywords:
Carbon corrosion
Electrolyte potential
Local fuel starvation
Startup/shutdown
Degradation
PEMFC

ABSTRACT

A two-dimensional model is developed to simulate the carbon corrosion reaction during operation of a Polymer Electrolyte Membrane fuel cell. Specifically, carbon corrosion caused by local fuel starvation and during a startup/shutdown (SUSD) procedure is investigated. The present model considers coupled transport of charged and non-charged species, and multiple electrochemical and chemical reactions. In the simulations, the same set of governing equations is solved for the local fuel starvation case and the SUSD case with appropriate boundary conditions and local properties applied to each case respectively. In the local fuel starvation case, a portion of the gas diffusion layer (GDL) is artificially set to have extremely low gas diffusivity in order to mimic the condition when locally the GDL is flooded by liquid water. For the SUSD case, a portion of the anode channel is filled with air, which simulates the purging/refilling in an SUSD procedure. Several mitigation techniques to reduce carbon corrosion are evaluated and it is found that for the local fuel starvation case, using OER (Oxygen Evolution Reaction)-favorable catalysts and using membranes with low O_2 diffusivity are two effective techniques for carbon corrosion mitigation. For the SUSD case, using OER-favorable catalysts appears to be the only effective mitigation technique.

1. Introduction

Polymer Electrolyte Membrane fuel cells (PEMFCs) have become a promising alternative energy source in the past decade, however, currently there are a few factors that delay the commercialization of them, e.g., cost of materials, hydrogen infrastructure, and material durability, etc. The issue of degradation of the membrane electrode assembly (MEA) materials is a major obstacle to wide adoption of these fuel cells. In the literature, several degradation modes have been identified for PEMFCs:

(1) Membrane degradation: Mechanical degradations such as membrane thinning and pinhole formations as a result of hydrolytic decomposition at elevated temperature and induced stresses, peroxide lead free radical attack and subsequent degradations are of more immediate importance due to potential of rapid irreversible damage [1]. Recently, there have been several publications that focused on the modelling aspect of membrane degradation. Shah et al. [2] developed a detailed model of chemical degradation of membrane. Their model considered the evolution of radicals, HF, carboxylic acid and CF2 groups. Their model also took into account the transport phenomena in the cell. Their model provides insights to the physico-electrochemical steps that lead to membrane degradation. Another recent report [3] proposed a 1D transient model as a simple evaluation tool for the effects of membrane permeability and relative humidity on cathode ionomer degradation, fluoride release and open circuit voltage degradation.

(2) Dissolution and migration of Pt particles: It has been confirmed experimentally that the Pt can be electro-oxidized at relatively high operational voltage. At the membrane/cathode interface, sufficient hydrogen flux (diffused from anode to cathode) chemically reduces oxidized platinum species, such as Pt^{2+}, in the ionomer phase, which then leads to nucleation and growth of platinum particles in the cathode ionomer phase, e.g., $Pt^{2+} + H_2 \rightarrow Pt + 2H^+$. Also the oxidized platinum species may move across the membrane and deposit on the anode layer in the absence of hydrogen in the anode compartment by the same reaction. The dissolution and migration of Pt particles could cause irreversible losses of electrochemical reaction area [4–6]. For modelling work on Pt dissolution and redeposition, Darling and Meyers [7] proposed kinetic expressions for the Pt oxidation and dissolution reactions and compared their simulation results with experimental data. The work by Bi et al. [8] reported a straightforward model to describe the formed Pt band location. Their work provided understanding of the physical process related to Pt dissolution and redeposition.

* Corresponding author. Tel.: +1 250 721 6288; fax: +1 250 721 6323.
E-mail address: jsui@uvic.ca (P.C. Sui).

0013-4686/$ – see front matter © 2009 Elsevier Ltd. All rights reserved.
doi:10.1016/j.electacta.2009.04.073

(3) Contamination of MEA due to poisoning: The effects of different contaminants on the performance degradation of PEMFCs have been investigated extensively. These contaminants include: fuel impurities (CO, CO_2, H_2S, and NH_3), air pollutants (NO_x, SO_x, CO, and CO_2), and cationic ions Fe^{3+} and Cu^{2+} resulting from the corrosion of fuel cell system components, e.g., from piping. These issues have been extensively reviewed by Cheng et al. [9]. For modelling work on contamination, Springer et al. [10] reported a refined interfacial kinetics to yield a better quantitative fit to the measured dependence of voltage loss on inlet CO level. Baschuk and Li [11] considered the effect of transport phenomena and oxygen crossover from cathode on CO poisoning. Shah et al. [12] reported a transient, fully two-phase, non-isothermal model of carbon monoxide poisoning and oxygen bleeding. The modelling work on contamination contribute to better understanding of kinetics and mechanism of contaminant poisoning and can be used to evaluate mitigation techniques for contaminant poisoning.

(4) Corrosion of carbon support in the catalyst layer due to local fuel starvation and startup/shutdown (SUSD) processes: Corrosion of the carbon support of catalysts is a major contributor to catalyst degradation. When carbon corrosion occurs, the carbon support in the catalyst layer is reduced in volume and connectivity and Pt particles may become isolated and less effective. The catalyst layer then suffers from reduction of electrochemical area (ECA), which leads to performance degradation.

In most research and development aimed at PEMFC durability thus far, much attention has been focused on the first three modes and less on the issue of carbon corrosion. For the topic of carbon corrosion, several experimental investigations have been reported by [13–15]. It has been confirmed experimentally that during local fuel starvation and SUSD process, the local cathode potential could rise to 1.2–1.5 V, which significantly speeds up the carbon corrosion [15]. An interesting recent paper [14] studied the mechanisms of carbon corrosion reactions (CCR). To the best of our knowledge, there are few papers focusing on modelling works of carbon corrosion [15–19]. These models are mostly limited to zero-dimensional or one-dimensional analysis, and the electrochemistry considered is not coupled with other transport processes such as oxygen through the membrane and transport of ion in the catalyst layer, which may play an important role in determining the carbon corrosion rate. More recently, Franco and Gerard [18] reported a mechanistic model on carbon corrosion reaction. Their model featured detailed electrochemistry and an explicit description of the instantaneous feedback between performance and the aging carbon support process. Another interesting recent paper was published by Takeuchi and Fuller [19], which presented carbon corrosion model induced by oxygen and hydrogen coexistence on the negative electrode. Their model captured the basic physics of carbon corrosion kinetics. As an application of their model, the effects of oxygen reduction exchange current and membrane thickness on carbon corrosion were discussed. For mitigating the carbon corrosion problem, several effective techniques have been reported: (1) use of catalysts that are favorable for the oxygen evolution reaction (OER), e.g., Pt-Ir/C [20]. (2) Use of membrane with low O_2 permeability to reduce O_2 crossover to anode [21]. (3) Use of corrosion resistant carbon support materials, e.g., graphitized carbon black [14]; (4) Increase of ionic conductivity of the catalyst layer. However, there have been few works published thus far on modelling and numerical simulations of these mitigation techniques and quantitative information of these mitigation techniques is lacking.

In the present study, we report on the development of a 2-D model for investigation of carbon corrosion caused by local fuel starvation and during SUSD scenario. In this model, transport of the reactant gases, proton and electron are solved in a coupled manner. Carbon corrosion kinetics is included in the model to predict the corrosion rate at cathodic catalyst layer of current reversal region. Furthermore, based on the models developed for local fuel starvation and SUSD, different mitigation techniques for carbon corrosion are investigated and evaluated numerically. The paper is organized as follows. First, the mathematical formulation of the problem is described, followed by the numerical methodology and implementation. In the Section 3, numerical results of two different cases (local fuel starvation and SUSD) are presented. For each case, our assessment on several mitigation techniques is discussed. The paper is concluded with a summary of findings and suggested future study.

2. Mathematical formulation of coupled transport and reactions

The mathematical formulation and numerical implementation of the coupled transport and reaction for carbon corrosion are described in this section. In essence, the conservation of gas species and charged species are solved for different region of the computational domain with appropriate boundary conditions prescribed for the events in consideration. The electrochemical and chemical reactions involved appear as the source/sink terms of the conservation equations. The corrosion process and most other electrochemical reactions depend strongly on local transport of gas species and charged species (ions and electrons), and vice versa. Therefore, it is necessary to couple them in the solution procedure. A two-dimensional configuration, i.e., in the direction along a straight gas channel and across the thickness direction of the MEA, is chosen for the present study because both the corrosion problems in question take place at least in both directions, therefore the transport in both directions need to be resolved.

2.1. Model assumptions

Several assumptions are made in the present model:

(1) The system reaches a steady or quasi-steady state. The process of corrosion is in general a time-dependent event, for instance, when carbon corrosion occurs in the catalyst layer, the carbon support is depleted, leading to a gradual decrease in overall cell performance. The SUSD process is time-dependent in nature. However, since the time scale of the corrosion process is considerably longer than most of other transport processes, e.g., mass transfer of species and electrical conduction, a quasi-steady state can be assumed.
(2) The system is isothermal. In typical cell designs and operation conditions, the unit cell has temperature variation within 10 °C, which is expected to affect reaction rates only slightly.
(3) Water is assumed to be in vapor phase in the entire domain. The impact of liquid water to carbon corrosion is neglected in the present study except that in the local fuel starvation case study, a portion of the GDL is assumed to be flooded by water.
(4) A constant ionic conductivity is assumed for the membrane and the catalyst layers. Assumptions (2)–(4) are made for the sake of simplicity; detailed modelling of non-ideal conditions can be found in Sui et al. [22].

2.2. Governing equations

The conservation equations of non-charged species (O_2 and H_2) and charged species (e^- and H^+) are solved in the computational domain. Table 1 lists the governing equations considered for different sub-domains. In these domains, since the transport of the species takes place in porous media where convection is minimal,

Table 1
Governing equations $-\nabla\cdot(D\nabla\phi)=S_\phi$.

Sub-domain	D	ϕ	S_ϕ
AGDL	$D_{O_2,\mathrm{eff}}$	C_{O_2}	0
	$D_{H_2,\mathrm{eff}}$	C_{H_2}	0
	σ_{solid}	ϕ_{solid}	0
	σ_{nafion}	$\phi_{\mathrm{electrolyte}}$	N/A
ACL	$D_{O_2,\mathrm{eff}}$	C_{O_2}	$i_{ORR}/4F-\dot{m}_{H-O}+i_{OER}/4F$
	$D_{H_2,\mathrm{eff}}$	C_{H_2}	$-i_{HOR}/2F-2\dot{m}_{H-O}$
	σ_{solid}	ϕ_{solid}	$-i_{HOR}-i_{ORR}-i_{OER}$
	σ_{nafion}	$\phi_{\mathrm{electrolyte}}$	$i_{HOR}+i_{ORR}+i_{OER}$
PEM	$D_{O_2,\mathrm{eff}}$	C_{O_2}	0
	σ_{nafion}	$\phi_{\mathrm{electrolyte}}$	0
CCL	$D_{O_2,\mathrm{eff}}$	C_{O_2}	$i_{ORR}/4F+i_{OER}/4F$
	σ_{solid}	ϕ_{solid}	$-i_{ORR}-i_{CCR}-i_{OER}$
	σ_{nafion}	$\phi_{\mathrm{electrolyte}}$	$i_{ORR}+i_{CCR}+i_{OER}$
CGDL	$D_{O_2,\mathrm{eff}}$	C_{O_2}	0
	σ_{solid}	ϕ_{solid}	0
	σ_{nafion}	$\phi_{\mathrm{electrolyte}}$	N/A

the governing equations for the transport are mostly diffusion equation with source terms.

2.3. Electrochemical kinetics

Four electrochemical reactions and one chemical reaction are considered in the present study, namely, the carbon corrosion reaction (CCR, I), hydrogen oxidant reaction (HOR, II), oxygen reduction reaction (ORR, III), oxygen evolution reaction (OER, IV) and hydrogen–oxygen chemical reaction (HOC, *V*):

$$C(s)+2H_2O\xrightarrow{CCR}CO_2+4H^++4e^- \quad (I)$$

$$H_2\xrightarrow{HOR}2H^++2e^- \quad (II)$$

$$O_2+4H^++4e^-\xrightarrow{ORR}2H_2O \quad (III)$$

$$2H_2O\xrightarrow{OER}O_2+4H^++4e^- \quad (IV)$$

$$2H_2+O_2\xrightarrow{Pt}2H_2O \quad (V)$$

Reactions (I)–(IV) are electrochemical reactions and their kinetics are assumed to follow the general form of the Butler–Volmer equation:

$$i_{RXN}=i_{0,RXN}\left[\prod_{\mathrm{Reactant}\,k}\left(\frac{C_k}{C_{k,\mathrm{ref}}}\right)^{\gamma_k}\right]\left\{\exp\left(\frac{\alpha_a F\eta}{RT}\right)-\exp\left(-\frac{\alpha_c F\eta}{RT}\right)\right\}\cdot\left(\frac{S}{V}\right)_{\mathrm{eff}}$$
$$RXN=\mathrm{CCR,HOR,ORR,OER} \quad (1)$$

where the overpotential is defined as

$$\eta=\phi_{\mathrm{solid}}-\phi_{\mathrm{electrolyte}}-V_{0,RXN} \quad (2)$$

The chemical reaction (HOC, *V*), is assumed to follow the common Arrhenius kinetics form dominated by oxygen concentration:

$$\dot{m}_{H-O}=k_{H-O}{C_{H_2}}^2C_{O_2} \quad (3a)$$

Since H_2 is abundant at anode side (for the local fuel starvation case) compared with the very small amount oxygen diffused from cathode to anode, the consumption of H_2 is neglected. The H_2 concentration term in Eq. (3a) can be treated as a constant:

$$\dot{m}_{H-O}(T)=k_{H-O}(T)\cdot C_{O_2};\quad T=343\,\mathrm{K} \quad (3b)$$

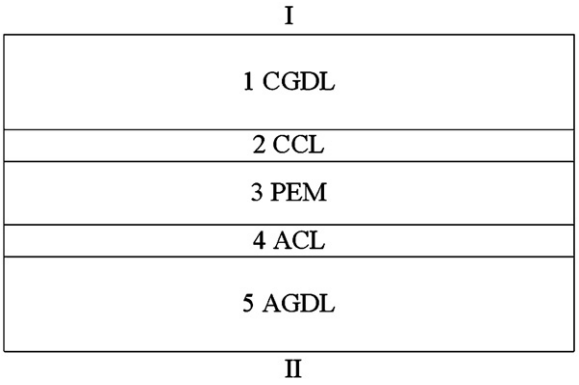

Fig. 1. Computational domain: 1 = cathode gas diffusion layer (CGDL), 2 = cathode catalyst layer (CCL), 3 = membrane (PEM), 4 = anode catalyst layer (ACL), 5 = anode gas diffusion layer (AGDL).

2.4. Numerical implementation

A straight, along-the-channel type of MEA domain is considered in the model, cf. Fig. 1. The computational domain has a length of 0.6 m. The thickness of the gas diffusion layer (GDL), catalyst layer (CL) and membrane is 250 μm, 25 μm and 50 μm, respectively. In Fig. 1, at boundary locations I and II (current collectors,) constant potential values and gas concentration are prescribed. All other boundary locations are set to be zero flux for all primary variables. The governing equations with the boundary conditions are solved using the multiphysics software COMSOL 3.3. The computational domain considered in the present study consists of 5960 elements, which is verified to yield grid-independent results.

2.4.1. Problem setup for simulation of carbon corrosion caused by local fuel starvation

Based on the methodology described in the previous sections, a computational model is constructed to simulate the transport and kinetics when locally the mass transport of a portion of the GDL is significantly hindered. This is simulated by arbitrarily assigning a low effective mass diffusivity to a patch in the computational domain. Specifically the patch of low diffusivity is located at $0.2\,\mathrm{m}\le x\le 0.3\,\mathrm{m}$ in the AGDL for the present study. In reality the low diffusivity zone may form because of flooding in the GDL or possibly the GDL surface in the gas channel is covered by immobile water droplets.

2.4.2. Problem setup for the SUSD simulations

For common operation of a stack, excess hydrogen is purged out of the stack by air flow during the shutdown stage in order to prevent fire hazard. The purging is usually performed with the electrical circuit shut off. During the shutdown process, however, internal current establishes within the stack due to the potential difference between the air portion and the hydrogen portion of the anode channel. The internal current in fact is a result of two reactions in both two portions of the cell, i.e., HOR/ORR in the hydrogen portion and ORR/CCR in the air portion, see the cartoon illustrated in Fig. 2. At the end of the shutdown procedure, the entire anode is filled with air and the internal current ceases. When the stack is restarted, hydrogen flow is introduced to the stack and the reverse phenomena in the shutdown process (internal current and carbon corrosion) take places.

A model is constructed to simulate the transport during the SUSD procedure. The setup of the model is similar to that described in Section 2.4.1 except in the boundary conditions for electrical conduction and gas concentration in the anode side of the domain. For the local fuel starvation model, cf. Section 2.4.1, the cell is connected

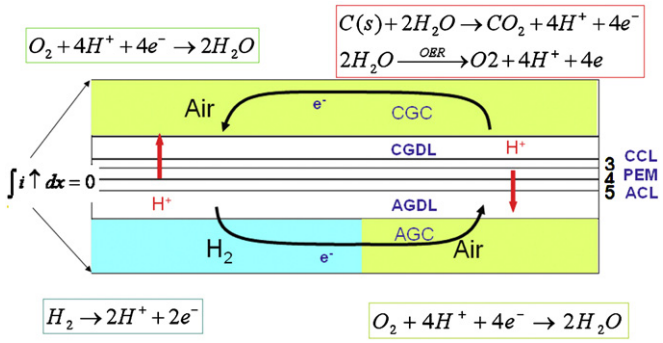

Fig. 2. Schematic for simulations on the SUSD process.

to an external load and a net current flow is resulted. In the SUSD model, the net current flow of electricity out of the cell is zero. However, internal current circulation is established due to the potential differential in the cell, as is illustrated in Fig. 2. In the SUSD model, a portion of the anode MEA boundary has hydrogen gas and the remaining portion of the MEA boundary is set to be air. The ratio of the portion filled with hydrogen versus air is arbitrarily chosen as 2:1.

In reference to Fig. 3, constant solid potentials and reactant concentrations are set to boundaries of CGDL and AGDL respectively:

Boundary I:

$$\begin{aligned} \phi_{\text{solid}} &= V(\text{OCV}) \\ C_{O_2} &= C_{O_2,0} \end{aligned} \tag{4}$$

Boundary II:

$$\begin{aligned} \phi_{\text{solid}} &= 0 \\ C_{H_2} &= C_{H_2,0} \end{aligned} \tag{5}$$

Boundary III:

$$\begin{aligned} \phi_{\text{solid}} &= 0 \\ C_{O_2} &= C_{O_2,0} \end{aligned} \tag{6}$$

The OCV potential on boundary I is not known *a priori*, and it is adjusted during the calculation until the zero net current condition is satisfied. Fig. 4 shows the flow chart of the solution procedure. The calculation first begins with an initial guess of the OCV. Then the transport and electrochemistry are solved based on the SUSD model. The OCV is gradually adjusted by step of 0.01 V starting from 1.1 V until a zero net current is achieved on the boundaries I and

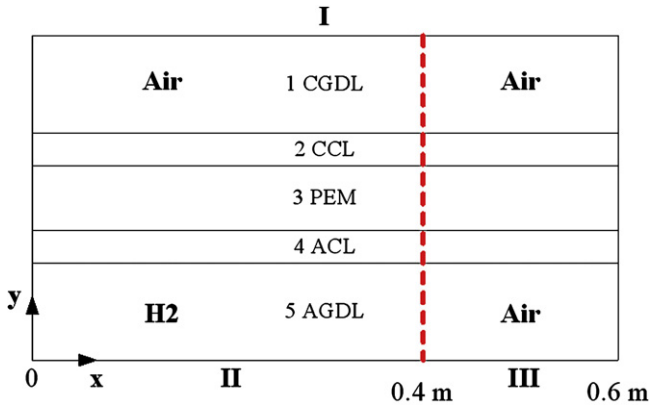

Fig. 3. Computational domain and boundary conditions for the USD model.

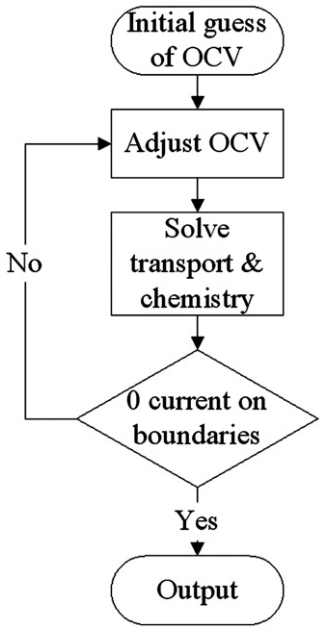

Fig. 4. Flow chart of the solution procedure for the SUSD model.

II + III, i.e., when

$$\int_{\text{I}} i_y \cdot \mathrm{d}x = 0 \tag{7}$$

$$\int_{\text{II+III}} i_y \cdot \mathrm{d}x = 0 \tag{8}$$

3. Results and discussion

Numerical results, including the baseline cases for local fuel starvation and the SUSD procedure and simulations on possible techniques for mitigation of carbon corrosion are discussed in the following.

3.1. Physical properties, dimensions for the baseline case

The transport properties of the baseline case are listed in Table 2. The kinetic parameters used in the simulation are listed in Table 3. The cell voltage for the baseline case is set to be 0.9 V. The effective oxygen diffusivity in the membrane phase is 1×10^{-9} m^2 s^{-1}. A specific area of 2000 m^{-1} is assumed in the catalyst layers. The cell is operated at pressure of 1 atm at 343 K and fully humidified gases (oxygen and hydrogen) are used.

3.2. Baseline results of the local fuel starvation case

The numerical results of the local fuel starvation case using the baseline properties and boundary conditions are shown below. The local fuel starvation case considers an anomalous condition when part of the cell is flooded and transport of oxygen into the catalyst layer is hindered. This perturbation not only decreases

Table 2
Transport properties for the baseline [22–26].

	σ_{H+}	σ_{e-}	ε	τ	D_{O_2}	D_{H_2}	$(S/V)_{\text{eff}}$
CL	5	50	0.4	1.5	4.2×10^{-5}	1.4×10^{-4}	2000
GDL	–	200	0.6	1	4.2×10^{-5}	1.4×10^{-4}	–
PEM	5	–	–	1.5	1×10^{-9}	–	–

Table 3
Kinetic parameters.

Reaction	Exchange current density, A m^{-3}	Anodic transfer coefficient	Cathodic transfer coefficient	Equilibrium potential, V	Concentration exponent
CCR	20	0.5	0.5	0.207	0
HOR	5×10^8	0.5	0.5	0	0.5
ORR	1×10^5	01	1.15	1	1
OER	500	1	1.15	1	0
HOC	$k_{H-O} = 540\ s^{-1}$ [25]				

According to [26], the diffusivity of CO through Nafion 112 was 0.7×10^{-9} m^2 s^{-1} (which is derived from the measured permeation). Since there is no data available for diffusivity of oxygen through membrane, in the present study we estimated it based on data obtained for CO and round it off to 10^{-9} m^2 s^{-1}.

cell performance but also cause carbon corrosion to occur in the vicinity of the local fuel starvation region.

3.2.1. Potential and current density distributions

Fig. 5 shows the predicted electrolyte potential, potential difference between the electrolyte and solid conductor, and current density at the interface of CCL and CGDL. The portion having a sudden change ($0.2\ m \le x \le 0.3\ m$) in these profiles is the simulated zone of local fuel starvation. It has been reported that at the interface between the normal and starvation regions, there is an abrupt decrease in the electrolyte potential [15]. This phenomenon is captured by the present model as shown in Fig. 5. One can see that the potential difference between the solid phase and the electrolyte phase in the starvation region increases to nearly 1.0 V. Such a high potential difference may cause significant carbon corrosion according to Eq. (1). In other word, the decrease in the electrolyte potential in the starvation region is the main driving force for the carbon corrosion reaction. From the current density profile in Fig. 5, it can be seen that at 0.9 V the current reversal behavior is clearly captured by the present model. The reversal current is estimated to ca. 250 A m^{-2} for the baseline case. The results show that significant amount of carbon can be depleted due to local fuel starvation.

3.2.2. Oxygen and hydrogen concentration distributions

Oxygen and hydrogen concentration distributions at GDL/Gas Channel (GC) for the baseline case are shown in Fig. 6. The differences of hydrogen and oxygen concentration between the normal region and the starvation region are observed. In the starvation region, oxygen concentration is higher than the normal region because CCR, instead of ORR, takes place in this region. It is noted that OER reaction also occurs in starvation region, which may increase oxygen concentration. Similarly in the starvation region, hydrogen concentration is lower than the normal region because part of the GDL is completely blocked by liquid water (by the artificial low diffusivity in this region). Consequently, the oxygen diffused from the cathode can hardly react with hydrogen. As a result, only ORR, rather than HOR, occurs in anode starvation region.

3.3. Mitigation techniques for carbon corrosion

From the simulation results discussed in the previous section, one can see that the carbon corrosion reaction tends to occur under certain conditions, namely, at high cell voltage and when oxygen is present in the anode side of the MEA. Therefore suppressing these conditions from occurring would likely reduce carbon corrosion. The electrochemical reaction (Eq. (1)) also provides clues to techniques that may help reduce carbon corrosion, e.g., by decreasing the exchange current density or overpotential between the electrolyte and the electron conductor, etc. Furthermore, from the multiple reaction pathways for ion generation, i.e., CCR versus OER, one can choose appropriate catalysts that favor OER against CCR to minimize the rate of carbon corrosion. Techniques based on these approaches for mitigation of carbon corrosion have been reported in the literature, e.g., [20–21]. In this section, numerical simulations are performed to gain insights to how these techniques would contribute to mitigation of carbon corrosion in typical MEA designs and cell operation. Table 4 lists the parameters used in the simulations for five different approaches discussed in the following.

3.3.1. Avoid operation of PEMFC near open circuit voltage region

Fig. 7 shows the prediction of reversal current density as a function of cell voltage for the baseline case. The reversal current in this figure is the total average current in the starvation region, which consists of contribution from both CCR and OER reactions. Breakdown of both currents can be seen Fig. 11(b). From Fig. 7, one can see

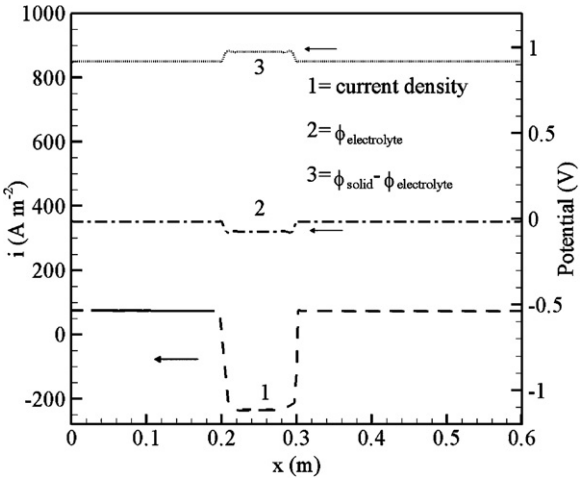

Fig. 5. Electrolyte potential ($\phi_{electrolyte}$), potential difference ($\phi_{solid} - \phi_{electrolyte}$) and current density profiles on the CCL/CGDL interface for cell voltage = 0.9 V.

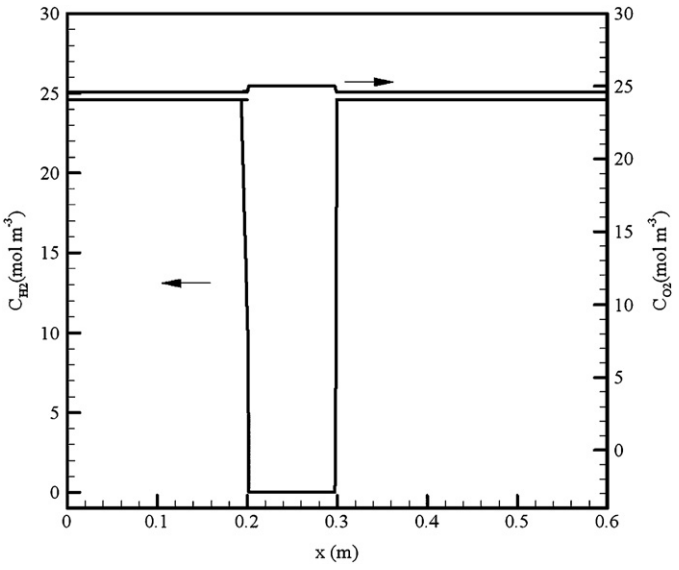

Fig. 6. Hydrogen and oxygen distributions for the baseline study at GDL/GC interfaces.

Table 4
Parameters used in simulations for different mitigation techniques.

	$(ai_0)_{OER}$ (A m^{-3})	$(ai_0)_{CCR}$ (A m^{-3})	$D_{O_2,PEM}$ (m^2 s^{-1})	σ_{PEM} (S m^{-1})
1	500	20	10^{-9}	5
2	**50000**	20	10^{-9}	5
3	500	20	**10^{-10}**	5
4	500	**1**	10^{-9}	5
5	500	20	10^{-9}	**20**

Bold values emphasizes the differences in parameters between baseline and other cases.

that the carbon corrosion rate remains high at higher cell voltage and a fall-off of the corrosion rate occurs for $V_{cell} < 0.5$ V. The dependence of the reversal current on cell voltage can be divided into two regions: at higher cell voltage ($V_{cell} > 0.5$ V), where the reversal current is high but insensitive to cell voltage; and the low cell voltage region ($V_{cell} < 0.5$ V), where the reversal current decreases as the cell voltage decreases. In the first region, the reversal current is determined mainly by the coupled ORR reaction at the cathode side of the starvation region, i.e., the reversal current is dictated by the diffusion of oxygen through membrane. This region is termed as the oxygen diffusion-limited region. In the second region, the reversal current is more dominated kinetically, i.e., the reversal current is determined by CCR overpotential. This region is termed as kinetics-limited region in the present study. In practice, when local fuel starvation occurs, switching the cell to operate at lower voltage is an effective method to mitigate carbon corrosion.

3.3.2. Use of membranes with low O_2 permeability

In the starvation region, the CCR at cathode side is strongly coupled with the ORR at anode side, therefore, O_2 diffusivity through membrane will have significant impacts on the carbon corrosion rate, especially in the oxygen diffusion-limited region. When the cell is operated at the kinetics-limited region, the effect of oxygen diffusivity has little effect on the reversal current because the reversal current is determined by kinetics rather than coupled oxygen diffusion in the starvation region. Fig. 8 shows the effects of O_2 diffusivity through membrane on average carbon corrosion rate. One can see that higher O_2 diffusivity results in higher carbon corrosion rate, thus using membranes having low O_2 diffusivity would be an effective way to mitigate carbon corrosion.

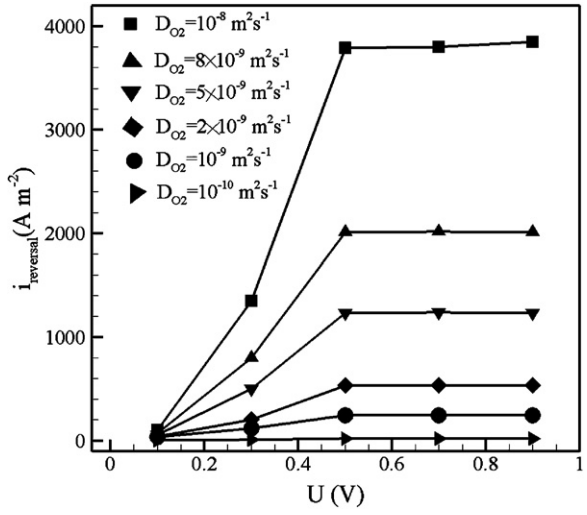

Fig. 8. Dependence of average carbon corrosion rate on O_2 diffusivity in membrane.

3.3.3. Use of corrosion-resistant carbon support

Fig. 9 shows the effects of carbon corrosion kinetics on the average carbon corrosion rate. The simulations were performed by varying the volumetric exchange current density in the reaction rate Eq. (1). One can see that higher volumetric exchange current density of CCR results in faster carbon corrosion rate, especially in the kinetics-limited region. In practice it is not easy to reduce the intrinsic volumetric exchange current density of CCR because $i_{0,c}$ (exchange current density with unit of A m^{-2}) is a constant for the reaction type and catalyst used. Alternatively a low carbon reaction rate can be achieved by reducing the surface-to-volume ratio (S/V). However, such practice may reduce other favorable reactions as well.

3.3.4. Increase of ionic conductivity of the catalyst layers

The effects of ionic conductivity in CLs on the average carbon corrosion rate are shown in Fig. 10. In general, higher ionic conductivity reduces the potential loss in the electrolyte, hence reduces the overpotential that drives carbon corrosion. An implication of

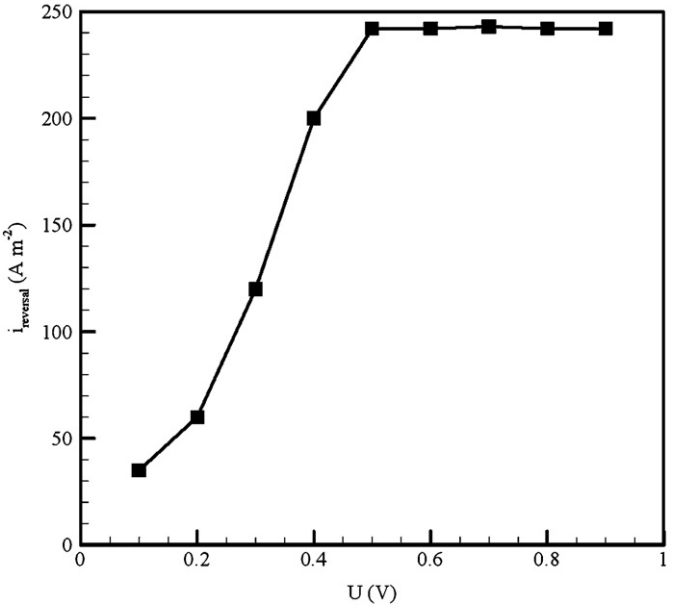

Fig. 7. Dependence of average carbon corrosion rate on cell voltage.

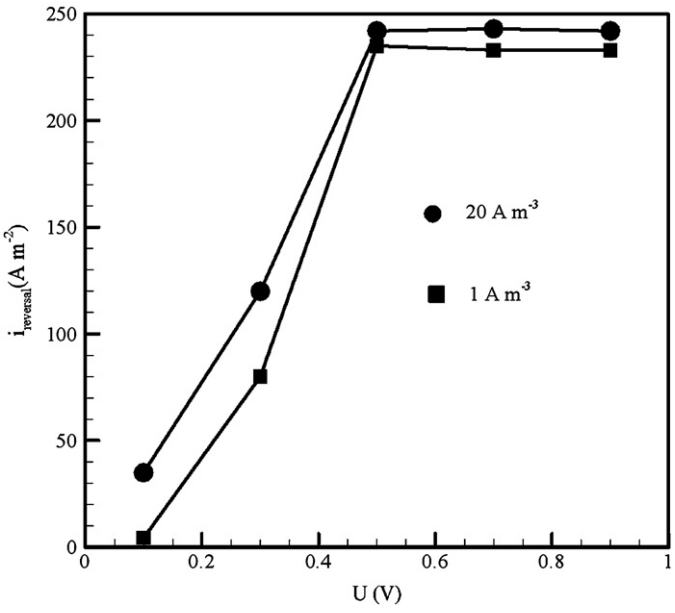

Fig. 9. Dependence of average carbon corrosion rate on carbon corrosion kinetics.

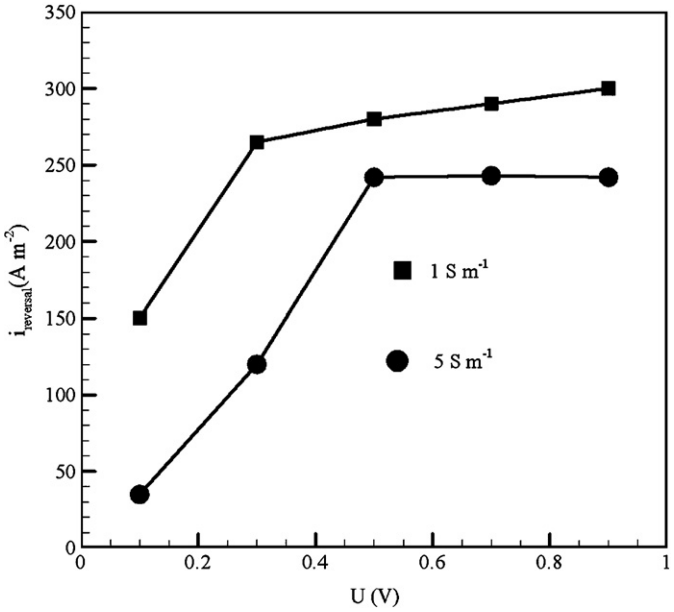

Fig. 10. Dependence of average carbon corrosion rate on ion conductivity of CL.

this simulation is that maintaining high water content in the CLs would be an effective for CCR mitigation.

3.3.5. Use of OER-favorable catalyst

Fig. 11(a and b) compare the simulation results using catalysts with high OER activity such as Pt-Ir/C versus Pt. The OER activity of the catalyst is adjusted by changing the OER volumetric exchange current density in the computation. From Fig. 11(a and b), one can see that for both cases the total reversal current is similar but the contribution on the CCR current differs significantly. The CCR current density is much lower when a high OER activity catalyst is used. This indicates that the CCR reaction is inhibited due to the OER reaction. It is noted that the OER reaction should have minimum impact to cell performance and durability. Therefore, if the reversal current caused by local fuel starvation is dominated by the OER current, cf. Fig. 11(a), degradation caused by CCR during local fuel starvation can be mitigated.

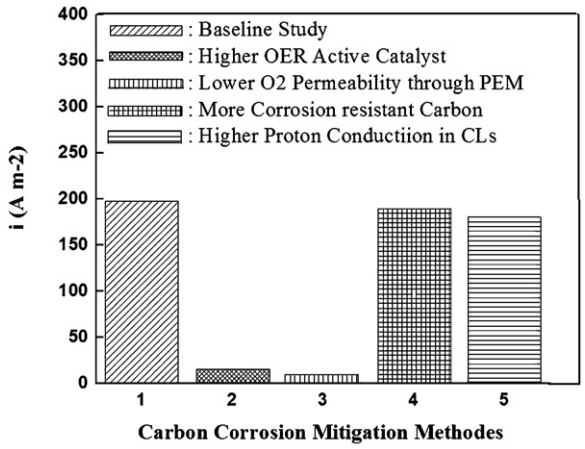

Fig. 12. Comparison of predicted reversal current for four CCR mitigation techniques.

3.3.6. Comparison of CCR mitigation techniques

Fig. 12 summarizes numerical results obtained using the baseline case for the four CCR mitigation techniques. One can see that using OER-favorable catalyst and using membrane of low O_2 permeability are two effective ways to mitigate carbon corrosion caused by local fuel starvation.

3.4. Baseline results of the SUSD model

The model shown in Fig. 3 is employed to investigate the transport during a SUSD procedure. Although in reality the SUSD procedure is a time-dependent process, in the numerical simulation, steady state solutions are obtained based on fixed boundary conditions. This implies that the characteristic time scale of the purging flow in the anode gas channel is much longer than most other transport processes in the domain and therefore a quasi-steady state assumption for these processes is valid.

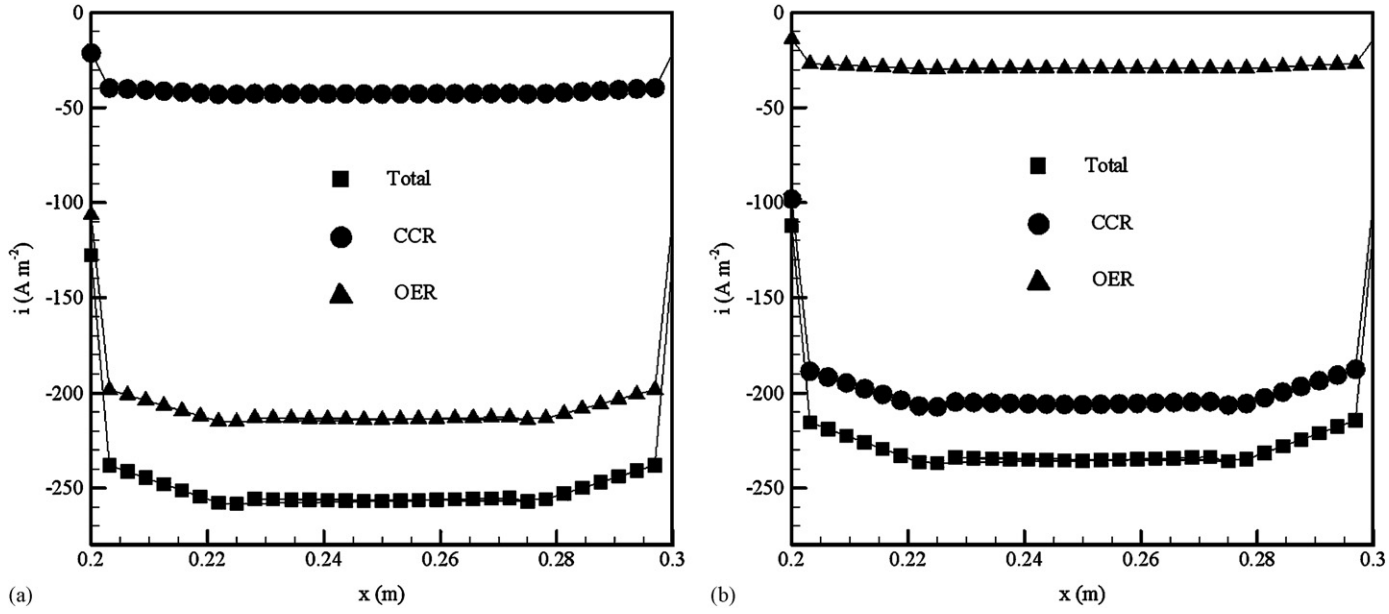

Fig. 11. (a) OER favorable catalyst, e.g., Pt-Ir/C, $ai_0 = 50{,}000\ A\,m^{-3}$ (b) Normal catalyst, $ai_0 = 500\ A\,m^{-3}$ for local fuel starvation.

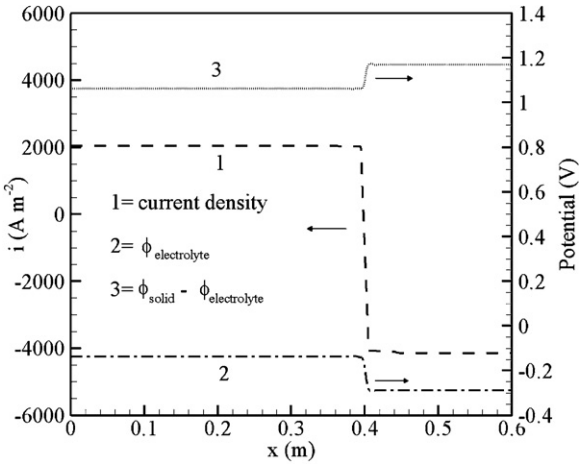

Fig. 13. Electrolyte potential, potential difference distribution and current density at CCL/CGDL interface for the baseline case.

3.4.1. Potential and current density distributions

Fig. 13 shows the electrolyte potential distribution, potential difference distribution and current density for the baseline case. The OCV value for this case is found to be 0.91 V in order to satisfy the zero net current boundary conditions as in Eq. (7) and (8). Similar to that observed in the local fuel starvation case discussed previously, an abrupt change in the electrolyte potential is seen at interface between H_2/Air and Air/Air portions, except that the amplitude of the electrolyte potential decrease is more pronounced in the SUSD case. This is due to the fact that in the SUSD process there is abundant oxygen on the anode side so that current reversal is amplified (ca. 4000 A m^{-2} versus 250 A m^{-2} in Fig. 5.) As a result, a larger potential difference (ca. 1.227 V in Fig. 13) is observed for the SUSD case, much higher than the maximum 1 V value for the local fuel starvation case, cf. Fig. 5.

3.5. Mitigation techniques of CCR caused by SUSD processes

Two of the mitigation techniques described in Section 3.3 are tested for the SUSD case to evaluate the effectiveness of these techniques. Similar to that observed in Section 3.3 for the local fuel starvation case, using OER-favorable catalyst, e.g., Pt-Ir/C and ai_0 = 50,000 A m^{-3}, cf. Fig. 14(a), is found to be a very effective way to reduce carbon corrosion. For the baseline case with normal catalysts, e.g., ai_0 = 500 A m^{-3}, carbon corrosion reaction contributes to the majority of the total current, cf. Fig. 14 (b). One can see that when an OER-favorable catalyst is used, the contribution of OER to the total reversal current increases significantly, thus carbon corrosion is inhibited.

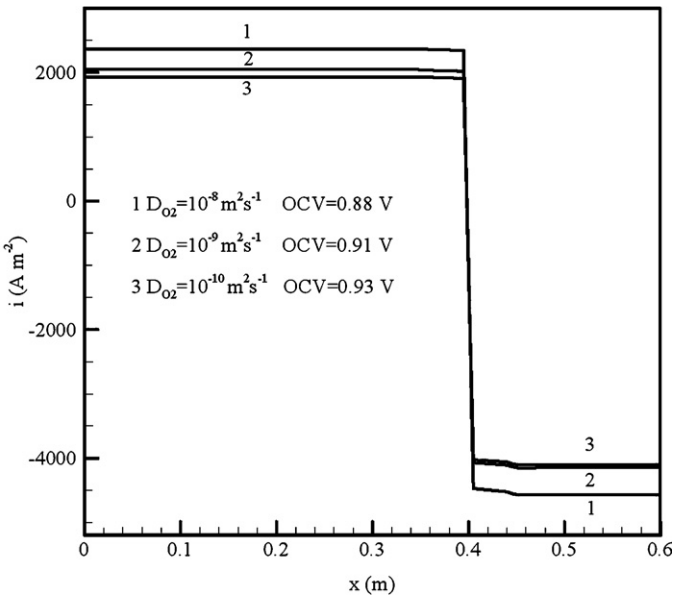

Fig. 15. Current density profile for different $D_{O_2,membrane}$.

Fig. 15 shows predicted current density profiles for different oxygen diffusivity through the membrane which varies over three orders of magnitude. One can see that the oxygen diffusivity has only slight effect on the reversal current. This observation for the SUSD case differs from that observed for the local fuel starvation case shown in Fig. 8. The explanation for this difference is that since there is abundant oxygen supply at anode side of reversal region (Air/Air region), the reversal reaction at cathode side

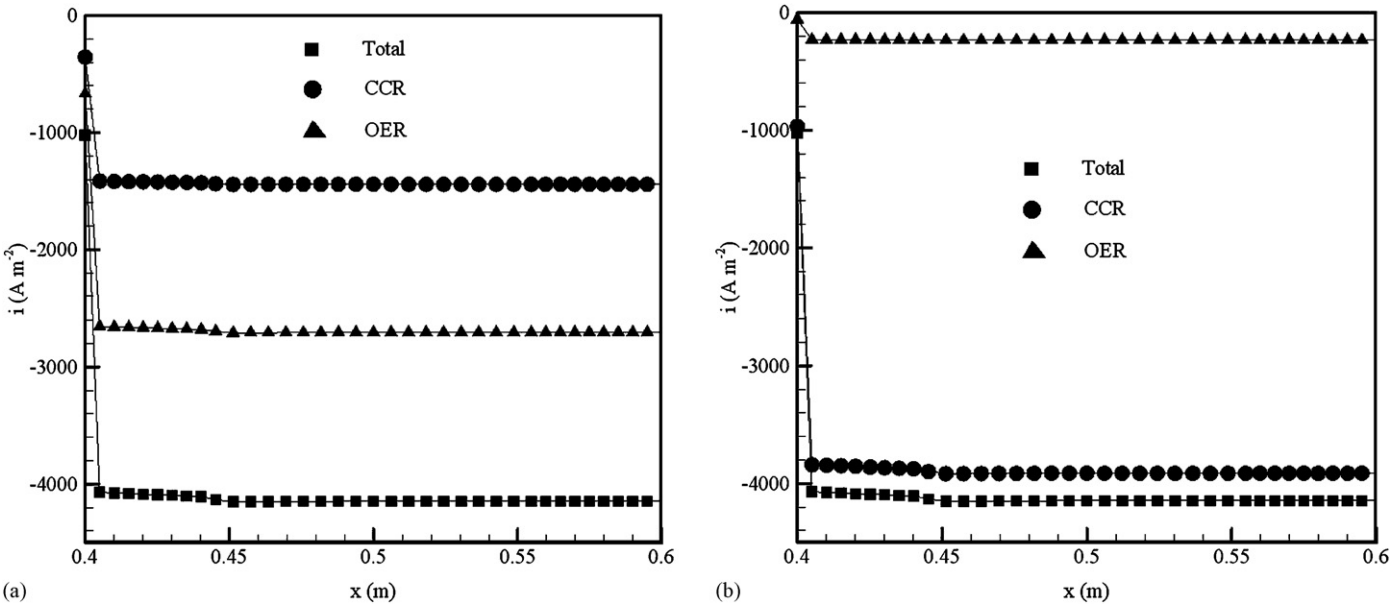

Fig. 14. Reversal current near the Air/Air and Air/H_2 interface (a) OER favorable catalyst and (b) Baseline catalyst.

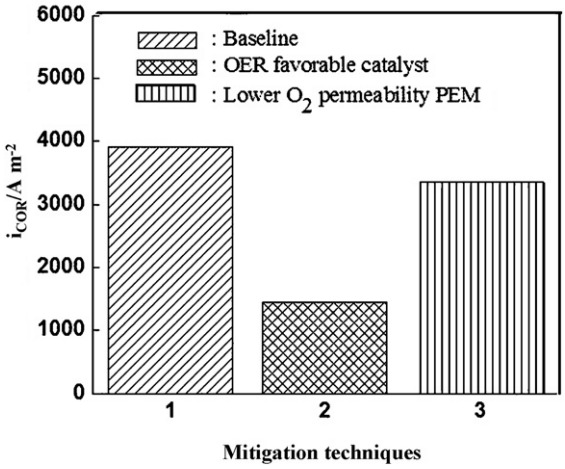

Fig. 16. Summary of numerical results for CCR mitigation techniques in an SUSD configuration. $(ai_{0,OER}, D_{O_2,PEM}) = (500,10^{-9})$ for Baseline, $(50,000,10^{-9})$ for Case 2, and $(500,10^{-10})$ for Case 3.

of the reversal region (Air/Air region) is less coupled with oxygen diffusion through the membrane. Therefore, oxygen diffusivity through membrane does not have much impact on CCR for the SUSD case.

Fig. 16 summaries the CCR mitigation techniques evaluated in the present study. Based on the simulation results, it is found that the CCR is accelerated for SUSD process and, CCR is only slightly affected by oxygen diffusion through the membrane. As a conclusion, only using OER-favorable catalyst is found to be an effective way for CCR mitigation for the SUSD process.

4. Conclusions

Modelling and numerical simulations on the coupled transport and electrochemical reactions related to carbon corrosion are reported in this study. A steady state model was developed to simulate carbon corrosion in a straight MEA configuration. The model takes into consideration the transport of charged species and gas species as well as a complete set of chemical and electrochemical reactions. The region where current reversal takes place is automatically manifested by the coupled solution procedure.

The present model was employed to investigate two scenarios, i.e., local fuel starvation and during startup/shutdown (SUSD) procedure. In the local fuel starvation case, it is found that the decrease of electrolyte potential at the interface between the normal region and the reversal region is the driving force of carbon corrosion reaction. The rate of carbon corrosion at the cathode side of the starvation region is found to be strongly dependent on oxygen diffusion through the membrane, whereas the effect of crossover oxygen for the SUSD is found to be relatively insignificant. Mitigation techniques of carbon corrosion for the local fuel starvation and the SUSD cases are investigated numerically. It was found that for local fuel starvation, using OER-favorable catalyst and low O_2 permeability membrane are two effective techniques for carbon corrosion mitigation. For SUSD, using OER-favorable catalyst appears to be the only effective mitigation technique due to the abundant oxygen at the reversal region. In the present local fuel starvation model, the local fuel starvation region (GDL blockage region) was designated and the rib-channel effect was not considered. In future study, the local fuel starvation model should be combined with two-phase model to predict the GDL blockage and liquid water surface coverage. Furthermore, the future study should investigate the effects in the in-plane direction and the difference of carbon corrosion under the channel and the rib. As for the startup–shutdown model, transient model should be implemented to address the transient behavior in the startup–shutdown process.

Acknowledgement

ND acknowledges the financial support in part from Ballard Power Systems.

Appendix A. Nomenclature

C_i	concentration for species (mol m^{-3})
D_i	diffusion coefficient (m^2 s^{-1})
F	Faraday constant (96487 C mol^{-1})
i	volumetric current density (A m^{-3})
i_0	exchange current density (A m^{-2})
$\dot{m}$	mass source terms (mol m^3 s^{-1})
R	universal gas constant (8.314 J mol^{-1} K^{-1})
S	general source term
S/V	surface-to-volume ratio (m^2 m^{-3})
T	temperature (K)
U	cell voltage (V)
x	axial direction of the channel (m)

Greek symbols

ε	porosity
Φ	general physical field (concentration, electrode, electrolyte)
ϕ	electrical potential
α	transfer coefficient
γ	concentration exponent
η	overpotential (V)

Subscript

a	anode
c	cathode
CCR	carbon corrosion reaction
eff	effective transport parameter
HOR	hydrogen oxidant reaction
Nafion	ionomer phase
OER	oxygen evolution reaction
OOR	oxygen reduction reaction
ref	reference state
solid	solid phase

References

[1] N. Ramaswamy, N. Hakim, S. Mukerjee, Degradation mechanism study of perfluorinated proton exchange membrane under fuel cell operating conditions, Electrochimica Acta 53 (8) (2008) 3279–3295.
[2] A.A. Shah, T.R. Ralph, F.C. Walsh, Modeling and simulation of the degradation of perfluorinated ion-exchange membranes in PEM fuel cells, Journal of the Electrochemical Society 156 (4) (2009) B465–B484.
[3] S. Kundu, M.W. Fowler, L.C. Simon, R. Abouatallah, N. Beydokhti, Degradation analysis and modeling of reinforced catalyst coated membranes operated under OCV conditions, Journal of Power Sources 183 (2008) 619–628.
[4] P.J. Ferreira, G.J. la, O.Y. Shao-Horn, D. Morgan, R. Makharia, S. Kocha, H.A. Gasteiger, Instability of Pt/C electrocatalysts in proton exchange membrane fuel cells—a mechanistic investigation, Journal of the Electrochemical Society 152 (11) (2005) A2256–A2271.
[5] K. Yasuda, A. Taniguchi, T. Akita, T. Ioroi, Z. Siroma, Platinum dissolution and deposition in the polymer electrolyte membrane of a PEM fuel cell as studied by potential cycling, Physical Chemistry Chemical Physics 8 (6) (2006) 746–752.
[6] J.W. Hu, H.M. Zhang, Y.F. Zhai, G. Liu, B.L. Yi, 500 h continuous aging life test on PBI/H_3PO_4 high-temperature PEMFC, International Journal of Hydrogen Energy 31 (13) (2006) 1855–1862.
[7] R.M. Darling, J.P. Meyers, Kinetic model of platinum dissolution in PEMFCs, Journal of the Electrochemical Society 150 (11) (2003) A1523–A1527.
[8] W. Bi, G.E. Gray, T.F. Fuller, PEM fuel cell dissolution and deposition in Nafion electrolyte, Electrochemical and Solid-State Letters 10 (5) (2007) B101–B104.

[9] X. Cheng, Z. Shi, N. Glass, L. Zhang, J.J. Zhang, D.T. Song, Z.S. Liu, H.J. Wang, J. Shen, A review of PEM hydrogen fuel cell contamination: Impacts, mechanisms, and mitigation, Journal of Power Sources 165 (2) (2007) 739–756.
[10] T.E. Springer, T. Rockward, T.A. Zawodzinski, S. Gottesfeld, Model for polymer electrolyte fuel cell operation on reformate feed effects of CO, H_2 dilution and high fuel utilization, Journal of the Electrochemical Society 148 (1) (2001) A11–A23.
[11] J.J. Baschuk, X.G. Li, Carbon monoxide poisoning of proton exchange membrane fuel cells, International Journal of Energy Research 25 (2001) 695–713.
[12] A.A. Shah, P.C. Sui, G.-S. Kim, S. Ye, A transient PEMFC model with CO poisoning and mitigation by O_2 bleeding and Ru-containing catalyst, Journal of Power Sources 166 (2007) 1–21.
[13] S. Maass, F. Finsterwalder, G. Frank, R. Hartmann, C. Merten, Carbon support oxidation in PEM fuel cell cathodes, Journal of Power Sources 176 (2) (2008) 444–451.
[14] K.H. Kangasniemi, D.A. Condit, T.D. Jarvi, Characterization of vulcan electrochemically oxidized under simulated PEM fuel cell conditions, Journal of the Electrochemical Society 151 (4) (2004) E125–E132.
[15] C.A. Reiser, L. Bregoli, T.W. Patterson, J.S. Yi, J.D.L. Yang, M.L. Perry, T.D. Jarvi, A reverse-current decay mechanism for fuel cells, Electrochemical and Solid-State Letters 8 (6) (2005) A273–A276.
[16] J.P. Meyers, R.M. Darling, Model of carbon corrosion in PEM fuel cells, Journal of the Electrochemical Society 153 (8) (2006) A1432–A1442.
[17] W.B. Gu, R.N. Carter, P.T. Yu, H.A. Gasteiger, Start/stop and local H_2 starvation mechanisms of carbon corrosion: model vs. experiment, ECS Transactions 11 (2007) 963–973.
[18] A.A. Franco, M. Gerard, Multiscale model of carbon corrosion in a PEFC: coupling with electrocatalysis and impact on performance degradation, Journal of the Electrochemical Society 155 (4) (2008) B364–B367.
[19] N. Takeuchi, T.F. Fuller, Modeling and investigation of design factors and their impact on carbon corrosion of PEMFC electrodes, Journal of the Electrochemical Society 155 (7) (2008) B770–B775.
[20] S.D. Song, H.M. Zhang, X.P. Ma, Z.G. Shao, Y.N. Zhang, B.L. Yi, Bifunctional oxygen electrode with corrosion-resistive gas diffusion layer for unitized regenerative fuel cell, Electrochemistry Communications 8 (3) (2006) 399–405.
[21] S.S. Kocha, J.D.L. Yang, J.S. Yi, Characterization of gas crossover and its implications in PEM fuel cells, AIChE Journal 52 (5) (2006) 1916–1925.
[22] P.C. Sui, S. Kumar, N. Djilali, Advanced computational tools for PEM fuel cell design Part 1. Development and base case simulations, Journal of Power Sources 180 (1) (2008) 410–422.
[23] S. Um, C.Y. Wang, Computational study of water transport in proton exchange membrane fuel cells, Journal of Power Sources 156 (2) (2006) 211–223.
[24] W. Sun, B.A. Peppley, K. Karan, Modeling the influence of GDL and flow-field plate parameters on the reaction distribution in the PEMFC cathode catalyst layer, Journal of Power Sources 144 (1) (2005) 42–53.
[25] M.C. Shao, S.L. Hu, Q.F. Wu, Study of the recombination of H_2 and O_2 at ambient temperature, J. Nuclear and Radiochemistry 24 (2002), 129-133 178.
[26] D.-W. Lee, S.-E. Nam, B. Sea, S.-K. Lim, K.-H. Lee, Permeation behavior of a H_2/CO gaseous mixture through Pt-included composite membranes, Journal of Membrane Science 243 (2004) 243–251.